





Extraction–Pyrolytic Method for TiO₂ Polymorphs Production

Vera Serga ^{1,2}, Regina Burve ^{1,2}, Aija Krumina ¹, Marina Romanova ³, Eugene A. Kotomin ² and Anatoli I. Popov ^{2,*}

¹ Institute of Inorganic Chemistry, Faculty of Materials Science and Applied Chemistry, Riga Technical University, Paula Valdena 3/7, LV-1048 Riga, Latvia; vera.serga@rtu.lv (V.S.); regina.burve@rtu.lv (R.B.); aija.krumina_4@rtu.lv (A.K.)

² Institute of Solid-State Physics, University of Latvia, Kengaraga 8, LV-1063 Riga, Latvia; kotomin@latnet.lv

³ Institute of Biomedical Engineering and Nanotechnologies, Riga Technical University, Viskalu 36A, LV-1006 Riga, Latvia; marina.romanova@rtu.lv

* Correspondence: popov@latnet.lv

Abstract: The unique properties and numerous applications of nanocrystalline titanium dioxide (TiO₂) are stimulating research on improving the existing and developing new titanium dioxide synthesis methods. In this work, we demonstrate for the first time the possibilities of the extraction–pyrolytic method (EPM) for the production of nanocrystalline TiO₂ powders. A titanium-containing precursor (extract) was prepared by liquid–liquid extraction using valeric acid C₄H₉COOH without diluent as an extractant. Simultaneous thermogravimetric analysis and differential scanning calorimetry (TGA–DSC), as well as the Fourier-transform infrared (FTIR) spectroscopy were used to determine the temperature conditions to fabricate TiO₂ powders free of organic impurities. The produced materials were also characterized by X-ray diffraction (XRD) analysis and transmission electron microscopy (TEM). The results showed the possibility of the fabrication of storage-stable liquid titanium (IV)-containing precursor, which provided nanocrystalline TiO₂ powders. It was established that the EPM permits the production of both monophasic (anatase polymorph or rutile polymorph) and biphasic (mixed anatase–rutile polymorphs), impurity-free nanocrystalline TiO₂ powders. For comparison, TiO₂ powders were also produced by the precipitation method. The results presented in this study could serve as a solid basis for further developing the EPM for the cheap and simple production of nanocrystalline TiO₂-based materials in the form of doped nanocrystalline powders, thin films, and composite materials.

Keywords: titanium dioxide; anatase; rutile; polymorphs; extraction–pyrolytic method



Citation: Serga, V.; Burve, R.; Krumina, A.; Romanova, M.; Kotomin, E.A.; Popov, A.I. Extraction–Pyrolytic Method for TiO₂ Polymorphs Production. *Crystals* **2021**, *11*, 431. <https://doi.org/10.3390/cryst11040431>

Academic Editors: Anton Meden, Philip Lightfoot and Pier Carlo Ricci

Received: 17 February 2021

Accepted: 14 April 2021

Published: 16 April 2021

Publisher's Note: MDPI stays neutral with regard to jurisdictional claims in published maps and institutional affiliations.



Copyright: © 2021 by the authors. Licensee MDPI, Basel, Switzerland. This article is an open access article distributed under the terms and conditions of the Creative Commons Attribution (CC BY) license (<https://creativecommons.org/licenses/by/4.0/>).

1. Introduction

Among many functional nanomaterials, nanocrystalline titanium dioxide (TiO₂) powders are of great interest due to their unique properties and numerous practical applications [1–11].

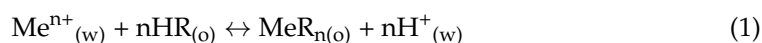
The current interest in titanium dioxide-based nanostructured materials is primarily associated with their high-tech applications: solar cells (dye-sensitized, quantum dots-sensitized and perovskite), lithium-ion batteries, supercapacitors, gas sensors and, etc. [1–5,12]. Moreover, active investigations are related to the photocatalytic activity of TiO₂-based materials, including nanopowders and thin films. Due to chemical stability, non-toxicity, low cost, and high availability, titanium dioxide is considered the most promising photocatalyst for the degradation of organic pollutants in water and air, as well as for water splitting and hydrogen production [1–3,7,8,13–19]. However, TiO₂ is a wide bandgap semiconductor (3.2 and 3.02 eV for the anatase and rutile phases, respectively [20]) that requires UV light (5% in the solar spectrum) for its activation. To reduce the bandgap, TiO₂ should be either doped (e.g., with N, Ta) or used in the form of nanotubes [13,21–26]. Other important studies are related to the applications of TiO₂ as protective coatings in microelectronic and optical devices and as luminescent compounds [27–32].

TiO₂ forms three naturally occurring polymorphic crystalline modifications in the form of the corresponding minerals: brookite with rhombic, anatase and rutile with a tetragonal crystal lattice [1,4,33]. Rutile is the most thermodynamically stable modification. During heating, anatase and brookite irreversibly transform into rutile, and the stability of the crystalline modification depends on the size of its constituent crystallites [34,35]. Both the temperature of phase transformation and the properties of the produced nanostructured materials are largely determined by their manufacturing technology [36].

Highly dispersed titanium dioxide-based materials for various applications on a laboratory scale are produced by such well-known wet chemistry methods as sol–gel, microemulsion, precipitation, hydrothermal, solvothermal, electrochemical, sonochemical and microwave [2–5,9–11,21,22,25,26,37–42]. These methods allow fabricating TiO₂ nanostructures with different phase compositions and morphology, in particular as nanoparticles, nanorods, nanowires, nanotubes and mesoporous structures. The most promising and widely used method for producing TiO₂ is the sol–gel method [3–5,8,9,22,37,41,43], allowing obtaining TiO₂ powders with well-defined particle size and shape, excellent purity and homogeneity [37,43]. In the framework of the mentioned methods, inorganic salts (e.g., titanium tetrachloride TiCl₄) or organometallic compounds, such as metal alkoxides (e.g., titanium (IV) isopropoxide Ti[OCH(CH₃)₂]₄) are usually used as titanium-containing precursors. However, these compounds have high reactivity with water, which must be taken into account both during the material synthesis to ensure good reproducibility and during the follow-up storage. It should be mentioned that titanium alkoxides are expensive and not environmentally friendly.

Thus, to date, there is a huge number of publications presenting various methods for synthesizing highly dispersed titanium dioxide-based materials with a wide range of functional properties. Nevertheless, the current pace of technological development requires new synthesis approaches characterized by simplicity, ease of scaling, good reproducibility, use of inexpensive raw materials, and allowing the production of materials with the required characteristics. The extraction–pyrolytic method (EPM) could be considered as one of these new developments.

The EPM is used to fabricate homogeneous nanocrystalline powders and films of oxide materials for various purposes [44–48]. The EPM belongs to wet chemistry methods. Using the EPM, the following steps are required: fabrication of extract (metal-containing precursor) via the method of exchange extraction by fatty (aliphatic monocarboxylic straight- or branched-chain) acids with the addition of alkali [49] and following thermal treatment—pyrolysis. This technique is quite simple, inexpensive and does not require complex equipment. One of the important advantages of the EPM is using organic extracts (solutions of metal carboxylates in a carboxylic acid or solvent) as metal-containing precursors. Such precursors are resistant to humidity and do not crystallize during long-term storage. In addition, high-purity inorganic metal salts are not required for their preparation. During liquid extraction, the target component is purified from impurities. The liquid extraction of metal ions by monocarboxylic acid (HR) proceeds via a cation exchange mechanism and can be generally represented by Equation (1):



where the subscripts w and o denote the aqueous and organic phases, respectively.

Alkali is added to the extraction system to increase the efficiency of target metal extraction since monocarboxylic acids themselves (with or without a diluent) are usually ineffective extractants [49].

To date, the EPM has already been applied for producing photoactive titanium dioxide films [45]. As the initial components for preparing the Ti-containing extract, the authors used an aqueous solution of titanium (IV) oxysulfate TiOSO₄ and α-branched monocarboxylic acids of C₅–C₉ fractions as an extractant.

The aim of this work is to develop the EPM for the production of nanocrystalline TiO₂ powders using valeric acid-based extracts; and to study the effect of pyrolysis conditions

on the phase composition, the mean crystallite size, and morphology of the fabricated materials. In addition, the results acquired by the EPM are compared with those related to the simplest and widely known production method—precipitation. In both approaches, the initial components are a freshly prepared aqueous solution of titanium (III) chloride as a titanium source and an aqueous solution of sodium hydroxide as an alkaline agent.

2. Materials and Methods

2.1. Preparation of the Precursors

2.1.1. Preparation of Aqueous Solution of Titanium (III) Chloride TiCl_3

An aqueous solution of TiCl_3 in diluted hydrochloric acid HCl with a metal concentration of 0.1 M was used as a titanium source. It was prepared immediately before both extraction and precipitation. For this, 1.200 g of titanium powder (particle size $d = 63\text{--}100\ \mu\text{m}$) was dissolved in 60 mL of HCl solution (1:1) during heating until the metal was completely dissolved. Thereafter, the solution was cooled down and diluted with distilled water to a volume of 250 mL.

2.1.2. Preparation of Titanium-Containing Precursors (E) via Liquid–Liquid Extraction

Valeric acid $\text{C}_4\text{H}_9\text{COOH}$ without diluent was used as an extractant. During preparing the precursor E1, the initial ratio of the volumes of the aqueous (V_w) and organic (V_o) phases in the extraction system was 3:1. For the extraction, the extractant and TiCl_3 solution (pH ~ 0.65) were placed in a separatory funnel, and 1 M NaOH solution was added step-by-step. When the organic phase (extract) turned deep blue, the addition of alkali was stopped. After a clear phase separation (~ 10 min), the aqueous phase was removed from the funnel, and its pH value was around 1.15. The organic phase was filtered through a cotton filter to remove water droplets.

To increase the titanium content in the organic phase for preparing the precursor E2, the initial $V_w:V_o$ ratio was taken as 5:1. The metal was extracted from TiCl_3 solution with a pH value of ~ 0.74 . Moreover, the addition of an alkaline solution was continued until a saturated solution of titanium valerate $\text{Ti}(\text{C}_4\text{H}_9\text{COO})_3$ in valeric acid was obtained, i.e., a finely dispersed precipitate appeared in the organic phase. As a result, the achieved pH value of the aqueous phase after extraction was about 1.23. To separate a small amount of the formed precipitate and to obtain a true solution, the organic phase was filtered through a double thick paper filter.

2.1.3. Preparation of Titanium-Containing Precursor (P) via Precipitation

As the first step, alkaline hydrolysis of TiCl_3 solution was carried out at room temperature. 0.5 M NaOH solution was added dropwise (at a rate of ~ 3 mL/min) under vigorous stirring until the pH of the aqueous phase reached ~ 6.0 . Then, the mixture was left to stay for a day. This was followed by filtration, multiply washing of the resulting precipitate with distilled water (the presence of chloride ions in the decanted solution was controlled with an AgNO_3 solution) and, after all, with ethanol. The precipitate was dried at room temperature for 36 hours, ground in an agate mortar and used as a precursor (P).

2.2. Thermal Treatment of Precursors

The resulting precursors E1 and E2, as solutions, and precursor P as powder were heated from room temperature to $350\text{--}750\ \text{°C}$ at a heating rate of $10^\circ/\text{min}$, annealed for an hour and rapidly cooled down under ambient conditions. Such thermal treatment was performed in laboratory furnace SNOL 8.2/1100. Thereafter, the produced samples were ground by pestle in an agate mortar and collected. For further investigations, only as-prepared powders without any additional posttreatment were used.

2.3. Characterization Methods

The metal concentration in the resulting precursors E was determined by the gravimetric method [50].

The thermal behavior of all the produced precursors was studied by simultaneous thermogravimetric analysis and differential scanning calorimetry (TGA–DSC) using the STA PT1600 (LINSEIS). The samples under test were heated from room temperature to 700 °C or 1000 °C at a rate of 10°/min in the static air atmosphere.

The phase composition of the produced materials was investigated by the X-ray diffraction (XRD) method (diffractometer D8 Advance, Bruker Corporation) with CuK α radiation ($\lambda = 1.5418 \text{ \AA}$). The XRD patterns were referenced to the PDF ICDD 00-021-1272 for anatase phase of TiO₂, PDF ICDD 00-021-1276 for rutile phase of TiO₂, and PDF ICDD 00-014-0277 for sodium polytitanate (Na₂Ti₆O₁₃) identification. The mean crystallite size (d) of the titanium dioxide was defined from the half-width of the diffraction peaks (101) of anatase (d_A) and (110) one of rutile (d_R) by the Scherrer method (EVA software). The weight fraction of the rutile phase (W_R) was determined by Gribb and Banfield [34] using integrated intensities A (areas) of the most intense diffractions peaks as follows (Equation (2)).

$$W_R = \frac{A_R}{0.884A_A + A_R} \cdot 100\% \quad (2)$$

IR spectra were recorded at room temperature using Bruker Tensor II FTIR spectrometer at a resolution of 4 cm⁻¹ and 36 scans for each spectrum. TiO₂ powder was mixed with KBr, and the pellets with a 7 mm diameter were prepared using Specac Mini-Pellet press under a load of 2000 kg. The morphology of the samples was examined by transmission electron microscopy (TEM) (FEI Tecnai G2 F20 operating at 200 kV).

3. Results

3.1. Precursors Characterization

Titanium-containing precursors (E) During extraction, Ti³⁺ cations are transferred from the aqueous phase into the organic phase as Ti(C₄H₉COO)₃, and the organic solution gradually turns deep blue. As a result of the storage of the produced titanium-containing extract E1 in a glass flask, the organic solution underwent discoloration, first, gradually and after ~60 minutes complete. The process was likely associated with the oxidation of Ti (III) to Ti (IV) by atmospheric oxygen. To our knowledge, there is no data on the composition of the final titanium (IV) carboxylate formed this way in an organic solution. However, it can be assumed that this compound may have the following composition: Ti(C₄H₉COO)₄ and/or (C₄H₉COO)₃TiOTi(OOCC₄H₉)₃.

Note that the discoloration of the organic titanium-containing extract E2 was observed already during filtration. According to the results of the gravimetric analysis, the titanium concentration in the precursors E1 and E2 was 0.14 M and 0.50 M, respectively.

Thus, colorless transparent organic solutions with different titanium concentrations were prepared. Upon storage of E1 and E2 precursors in glass flasks with ground-glass stoppers at room temperature, no changes in color and transparency (homogeneity) were observed.

Titanium-containing precursor (P) As a result of the produced precipitate (gel) storage during the day, its color changed from deep gray-blue to white because of the oxidation of titanium (III) hydroxide by atmospheric oxygen and the formation of hydrated titanium dioxide (titanium oxyhydrate) TiO₂·nH₂O [51].

3.2. Thermal Behavior of Precursors E1, E2, and P

The main thermal decomposition products of the salts of many carboxylic acids are ketones and the corresponding metal oxides, while the temperature of their decomposition is characteristic for each certain compound [52]. This is why the study of the thermal behavior of the extracts produced during the EPM (solutions of metal carboxylates in carboxylic acid or diluent) is rather important and necessary for determining the minimal pyrolysis temperature for the production of organic impurity-free oxide materials.

The results of TG-DSC analysis of liquid precursors E1 and E2 with different titanium concentrations are shown in Figure 1. According to the data presented, studied precursors

demonstrate similar thermal behavior during the heating process. At the same time, the thermal effects are more pronounced for the precursor with higher titanium concentration (E2) and just these results (see Figure 1B) will be discussed in detail.

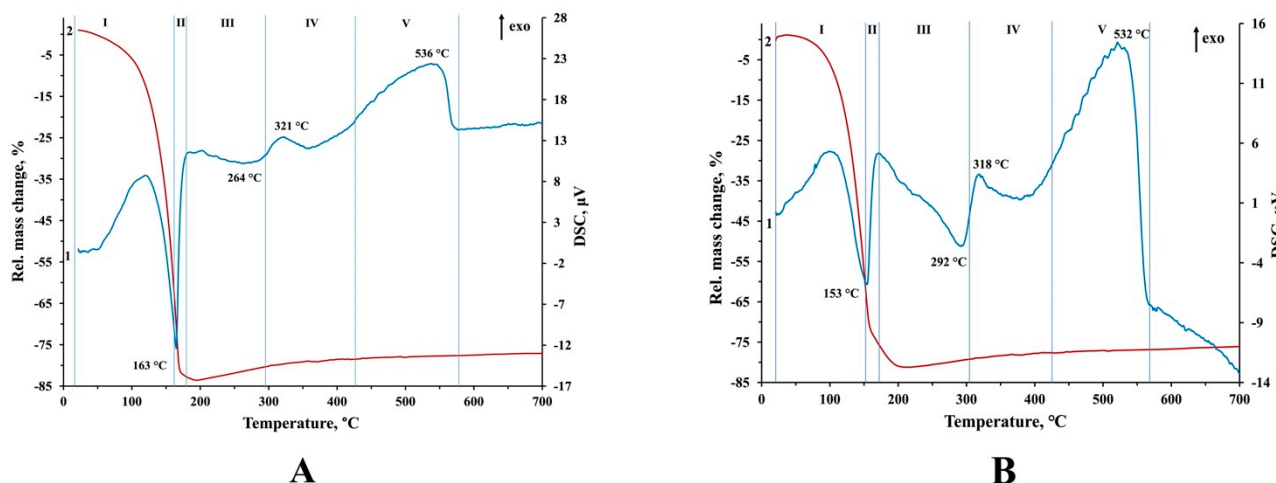


Figure 1. DSC (1) and TGA (2) curves of the precursors produced by extraction–pyrolytic method (EPM): (A) E1; (B) E2.

The precursor E2 is thermally stable up to a temperature of ~ 30 °C. The first endothermic peak on the DSC curve at ~ 153 °C is accompanied by active sample weight loss. In the temperature range from ~ 30 °C to ~ 153 °C (fragment I), this weight loss is mainly associated with the removal of free extractant (valeric acid) and co-extracted water, while at a further temperature increase (fragment II)—with the decomposition of the titanium (IV) carboxylate. The second broad asymmetric endothermic peak is observed at ~ 180 – 306 °C (fragment III). In the region of this peak, the decomposition of titanium carboxylate still continues and is followed by active evaporation of the organic decomposition product (probably, dibutyl ketone $C_4H_9COC_4H_9$ with $T_{\text{boiling}} = 182$ – 187 °C). According to the TG curve, the weight loss reaches $\sim 82\%$ at ~ 210 °C and stops. A further temperature rise to 700 °C is accompanied by a gradual increase in the sample weight by $\sim 4\%$. That is most likely associated with the gradual oxidation of titanium monoxide TiO to TiO_2 using the proposed in Ref. [53] decomposition mechanism of the metal (IV) carboxylate via the formation of metal monoxide as intermediate. Moreover, at ~ 210 – 300 °C, this process occurs simultaneously with the removal of volatile organic decomposition products. The increase in sample weight observed on the TG curve (Figure 1B, curve 2) shows that TiO oxidation is the dominant process. At the same time, the predominance of the endothermic evaporation process is observed as well (see curve 1 in Figure 1B). A weak exothermic peak at ~ 318 °C (fragment IV) on the DSC curve is caused by the combustion of gaseous organic residue. In the temperature range, ~ 433 – 561 °C (fragment V), an intense asymmetric exothermic peak assumes the superposition of several thermal effects: crystallization of an amorphous phase, anatase-to-rutile polymorphic transformation and pyrocarbon burnout. Thus, according to the analysis of the obtained results, it could be assumed that upon heating, the organic decomposition product (most likely, ketone) is removed after forming TiO and its oxidation to TiO_2 .

For comparison, the thermal behavior of a solid precursor P (titanium oxyhydrate sample) was also studied. The presented thermogram (Figure 2, curve 1) shows two endothermic and one exothermic peak. The endothermic effect observed at ~ 56 – 150 °C (fragment I) is accompanied by active weight loss ($\sim 20\%$) of the dried precipitate due to the removal of adsorbed water. With a further increase in temperature, the sample loses crystallization water. This process is accompanied by a wide endothermic peak at ~ 208 – 308 °C (fragment II) and a small weight loss ($\sim 5\%$). The intense exothermic peak at ~ 776 °C (fragment III) is associated with the crystallization of titanium dioxide and polymorphic

anatase-to-rutile transformation. Ongoing slight loss of sample weight is probably due to the continuation of the dehydration process.

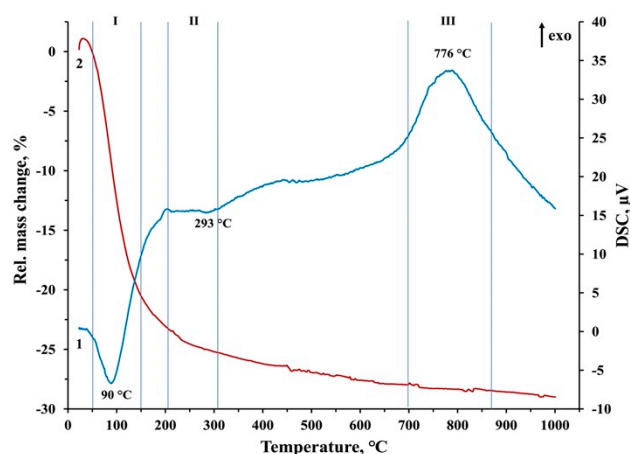


Figure 2. DSC (1) and TG (2) curves of the precursor (P).

According to Figures 1 and 2, due to the different chemical compositions, the thermal behavior of the studied precursors differs significantly. Thus, the observed weight loss of the precursor P upon heating is associated with successive dehydration processes. At the same time, thermal transformations in precursors E are associated with the complex decomposition of titanium carboxylate, which is preceded by the evaporation processes of the solvent (valeric acid) and co-extracted water being the parts of the extracts.

3.3. XRD Analysis

To obtain a solid final product from precursors E1 and E2, based on the TG-DSC results (see Figure 1), the minimal temperature of pyrolysis was chosen as 350 °C. To study the effect of the precursor preparation method on the phase composition, anatase-to-rutile transformation temperature, and the mean crystallite size of TiO₂, heat treatment of precursors E and P was carried out in the range from 450 °C to 750 °C with a temperature step of 100 °C. Table 1 summarizes the results of the XRD analysis of all the produced materials.

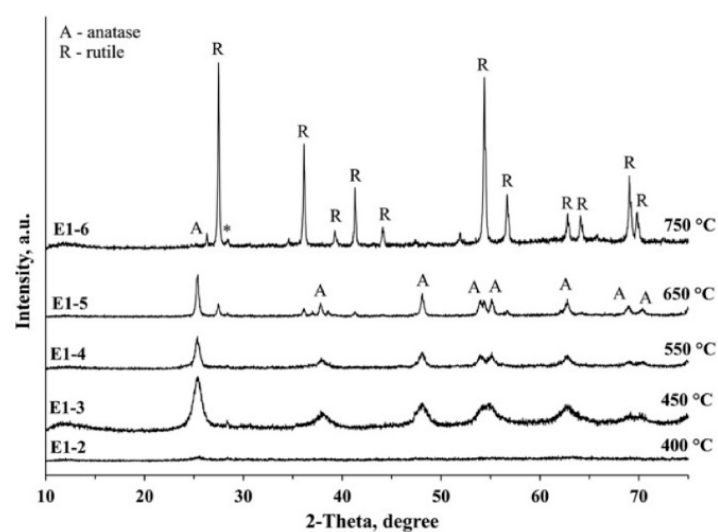
The study of the regularities of phase formation during the pyrolysis of the precursor E1 testifies (Figure 3, Table 1, samples E1-1–E1-6) that amorphous powders are produced at temperatures of 350 °C and 400 °C. The crystallization of anatase polymorph begins at 450 °C, while the polymorphic anatase-to-rutile transformation starts at 650 °C. TiO₂ powder produced at 750 °C contains rutile polymorph with only a small anatase admixture ($W_A = 1.1\%$).

According to the XRD analysis (Figure 4, Table 1, samples E2-1–E2-6), the heat treatment of a more concentrated precursor E2 at 400 °C corresponds to the beginning of the anatase phase crystallization. Pyrolysis of the precursor at 550 °C and 650 °C leads to the gradual polymorphic transformation of anatase to rutile with a simultaneous increase in the mean crystallite size of anatase from ~20 nm to ~35 nm and of rutile from ~30 nm to ~45 nm, respectively. As a result of heat treatment at 750 °C, a monophase product consisting of a rutile polymorph with $d_R \sim 53$ nm is formed.

Thus, an increase in titanium concentration in the precursor solution from 0.14 M to 0.50 M decreases the temperature of anatase-to-rutile transformation by ~100 °C (see Figures 3 and 4, Table 1).

Table 1. Impact of the heat treatment conditions of titanium-containing precursors on the phase composition and mean crystallite size of the final products.

Sample Nr.	Production Conditions		XRD Analysis Results		
	Precursor	Pyrolysis Temperature T_p , °C	Phase Composition	d , nm	W, %
E1-1	E1	350	Amorphous	-	-
E2-1	E2				
E1-2	E1	400	Amorphous	-	-
E2-2	E2		Anatase	5	100
E1-3	E1	450	Anatase	8	100
E2-3	E2		Anatase	9	100
P-1	P		Anatase	9	100
E1-4	E1	550	Anatase	15	100
E2-4	E2		Anatase Rutile	20 ~30	87.7 12.3
P2	P		Anatase	10	100
E1-5	E1	650	Anatase Rutile	30 ~40	80.9 19.1
E2-5	E2		Anatase Rutile	~35 45	20.6 79.4
P3	P		Anatase Rutile	14 Discerned	96.4 3.6
E1-6	E1	750	Anatase Rutile	Discerned 65	1.1 98.9
E2-6	E2		Rutile	53	100
P-4	P		Rutile $\text{Na}_2\text{Ti}_6\text{O}_{13}$	68 -	100 -

**Figure 3.** XRD patterns of nanocrystalline TiO_2 powders produced from the precursor E1 at different pyrolysis temperatures. * Signal of a silicon substrate from the measuring cuvette.

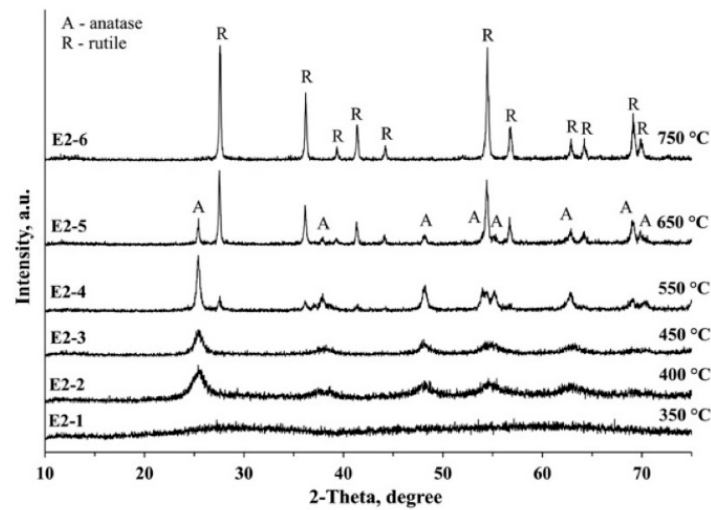


Figure 4. X-ray diffraction patterns of nanocrystalline TiO_2 powders produced from the precursor E2 at different pyrolysis temperatures.

According to XRD analysis, precursor P is amorphous (Figure 5, Table 1). The anatase phase, produced as a result of the heat treatment of precursor P, is similar to these at the precursor E1 treatment at 450 °C and 550 °C. The increase of the processing temperature to 650 °C or 750 °C leads to the formation of two phases of TiO_2 . Moreover, depending on the heat treatment temperature, either anatase or rutile is a dominating phase (Figure 5, samples P-3 and P-4). It was also found two processes occur simultaneously at 750 °C: the polymorphic transformation of anatase into rutile and the crystallization of the admixture phase, $\text{Na}_2\text{Ti}_6\text{O}_{13}$. This phase is a product of the interaction of NaOH with TiO_2 at high temperatures, i.e., during the preparation of a precursor P, it is impossible to completely remove the residual amounts of NaOH by washing the precipitate (gel). In the case of the EPM, a system of two immiscible liquids is used, and the target product (titanium carboxylate) is dissolved in the organic phase, while water-soluble reaction components, in the aqueous phase. Hence, the presence of impurity phases in the TiO_2 samples was not established (see Figures 3 and 4).

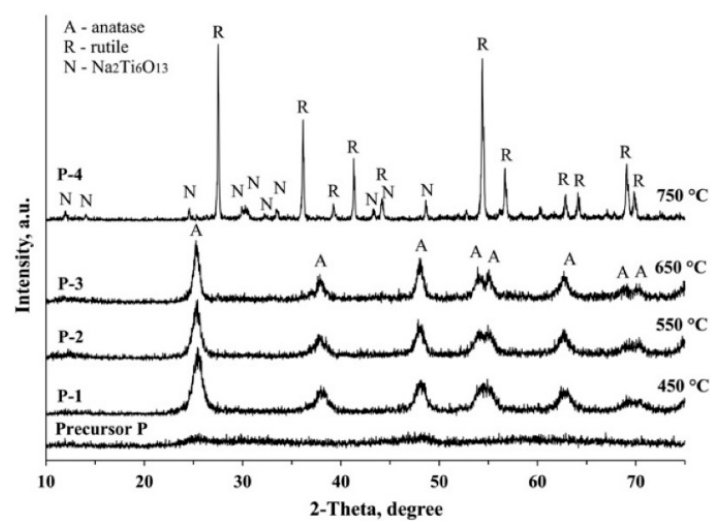


Figure 5. XRD patterns of nanocrystalline TiO_2 powders produced from the precursor P at different processing temperatures.

3.4. FTIR Spectroscopy

FTIR spectroscopy was used to determine the conditions for the thermal treatment of the precursor E2 that ensure complete removal of the organic component during TiO₂ production.

The FTIR spectra (see Figure 6) contain the peaks at 3449 cm⁻¹ and 1622 cm⁻¹, which correspond to the stretching and bending vibrations of –OH groups. Weak absorption bands at 2362 cm⁻¹ and 2332 cm⁻¹ in the samples are associated with the presence of carbon dioxide CO₂ adsorbed from the atmosphere [54]. In the case of the samples produced at 350 °C or 400 °C (Figure 6, samples E2-1 and E2-2), the spectra contain the absorption bands peaked at 1520 cm⁻¹ and 1375 cm⁻¹, which indicate the presence of undecomposed organic residue in these materials [55,56]. The presence of TiO₂ in the studied materials is confirmed by a wide absorption band at ~1000 cm⁻¹–400 cm⁻¹ associated with the vibrations of Ti–O–Ti bonds in the TiO₂ lattice [57,58]. In the mentioned spectral region, a shift of the maximum from 515 cm⁻¹ to 442 cm⁻¹ is observed upon the decrease in the precursor pyrolysis temperature from 550 °C to 350 °C (Figure 6, samples E2-4–E2-1). This fact may be related to the changes in the size of the produced TiO₂ particles, as described earlier in [41,59]. This is also consistent with the results of our XRD analysis (Table 1), under which a decrease in the pyrolysis temperature of the precursor E2 in this temperature range leads to a decrease in the mean crystallite size of anatase from 20 nm to 5 nm, and, finally, to amorphization. Thus, according to our results, to produce organic impurity-free TiO₂ powders via the EPM, the minimal pyrolysis temperature of the extracts (precursors E) should be 450 °C. The data obtained do not contradict the results of the TG-DSC analysis (Figure 1) presented above. A similar picture was observed at the comparison of the infrared spectra for bulk and nanosized AlN and LaPO₄ [60–62].

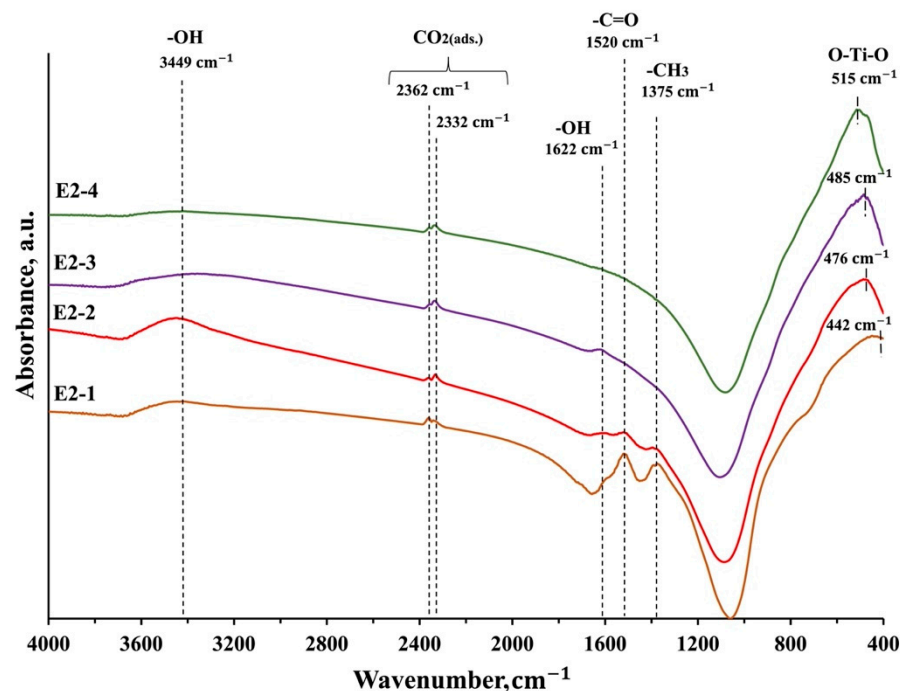


Figure 6. FTIR spectra of the samples produced from the precursor E2 at different pyrolysis temperatures: E2-1—350 °C, E2-2—400 °C, E2-3—450 °C, E2-4—550 °C.

3.5. Transmission Electron Microscopy

Figure 7 demonstrates TEM results for the anatase and rutile powders produced by the EPM and, for comparison, for the anatase sample produced by the precipitation method. According to the results obtained, the particles with irregular rounded shapes are formed as a result of the low-temperature treatment (450 °C) of both precursors (Figure 7A,C).

Nanoparticles with a mean size of ~ 8 nm can be observed that is in line with the XRD results ($d_A = 9$ nm, Table 1).

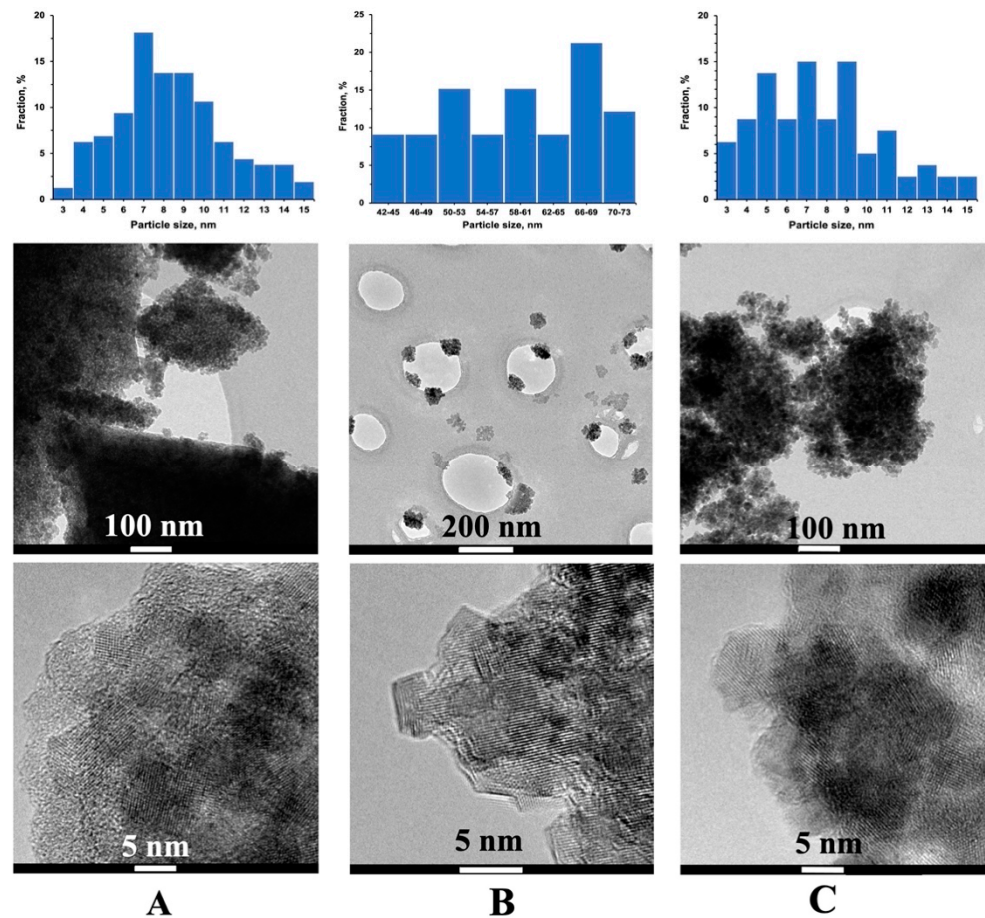


Figure 7. HR-TEM (a bottom row), TEM (a medium row) images and histograms of the particle size distribution (a top row) of samples produced by the EPM (A,B) and precipitation method (C) at temperatures: (A)—450 °C (sample E2-3); (B)—750 °C (sample E2-6); (C)—450 °C (sample P-1).

In the case of the EPM, the increase in the pyrolysis temperature up to 750 °C leads to the formation of layered aggregates consisting of the faceted particles with a mean size of ~ 11 nm (Figure 7B). It is possible that the formation of such structures is associated with the thermal behavior of the precursor upon heating (see Section 3.2), in particular, with the effect of the pyrolysis products of the organic precursor on the nanoparticle surface. The average size of the aggregates is about 58 nm that is consistent with the XRD data ($d_R = 53$ nm, Table 1).

4. Conclusions

This study suggests an original two-stage approach for synthesizing nanocrystalline TiO_2 powders—the extraction–pyrolytic method (EPM).

The conditions for preparing titanium-containing extracts (precursors) using valeric acid without a diluent as an extractant were determined. The minimum temperature of pyrolysis (450 °C) of the precursors for organic impurity-free nanocrystalline TiO_2 production was established. We have shown that the phase composition of the resulting powders is affected by the pyrolysis temperature and titanium concentration in the precursor solution. According to the XRD results, depending on pyrolysis conditions, the produced TiO_2 samples contain anatase ($d_A \sim 8$ –15 nm), mixed anatase-rutile or rutile ($d_R \sim 53$ nm) polymorphs. We have shown that the decrease in titanium concentration in the precursor solution from 0.50 to 0.14 M leads to the increase of the temperature of anatase-to-rutile polymorphic

transformation by ~ 100 °C. Comparative analysis of the results for the materials produced by two methods—the EPM and the precipitation, revealed some differences. According to the XRD data, as a result of the heat treatment at 750 °C, impurity phases were not detected in the EPM-produced materials, while the $\text{Na}_2\text{Ti}_6\text{O}_{13}$ impurity phase was identified in the material produced by the precipitation method.

The results presented in this study could serve as a solid basis for further developing the EPM for the cheap and simple production of nanocrystalline TiO_2 -based materials in the form of doped nanocrystalline powders, thin films and composite materials.

Author Contributions: Conceptualization, V.S. and A.I.P.; methodology, V.S. and R.B.; software, A.K. and M.R.; formal analysis, R.B., A.K. and M.R.; investigation, V.S. and R.B.; resources, E.A.K. and A.I.P.; data curation, E.A.K.; writing—original draft preparation, V.S., R.B. and A.I.P.; writing—review and editing, E.A.K. and A.I.P.; visualization, A.K. and M.R.; supervision, V.S. and A.I.P.; project administration, E.A.K.; funding acquisition, E.A.K. All authors have read and agreed to the published version of the manuscript.

Funding: This study was partly supported by the M-ERA.NET project SunToChem.

Institutional Review Board Statement: Not applicable.

Informed Consent Statement: Not applicable.

Data Availability Statement: Not applicable.

Acknowledgments: The authors thank V. Kuzovkov, A. Lushchik and M. Lushchik for many useful discussions. The research was (partly) performed in the Institute of Solid State Physics, University of Latvia ISSP UL. ISSP UL as the Center of Excellence is supported through the Framework Program for European universities Union Horizon 2020, H2020-WIDESPREAD-01–2016–2017-TeamingPhase2 under Grant Agreement No. 739508, CAMART2 project.

Conflicts of Interest: The authors declare no conflict of interest.

References

1. Gupta, S.M.; Tripathi, M. A review of TiO_2 nanoparticles. *Sci. Bull.* **2011**, *56*, 1639–1657. [[CrossRef](#)]
2. Ge, M.; Cao, C.; Huang, J.; Li, S.; Chen, Z.; Zhang, K.-Q.; Al-Deyab, S.S.; Lai, Y. A review of one-dimensional TiO_2 nanostructured materials for environmental and energy applications. *J. Mater. Chem. A* **2016**, *4*, 6772–6801. [[CrossRef](#)]
3. Macwan, D.P.; Dave, P.N.; Chaturvedi, S. A review on nano- TiO_2 sol-gel type synthesis and its applications. *J. Mater. Sci.* **2011**, *46*, 3669–3686. [[CrossRef](#)]
4. Dubey, R.S.; Krishnamurthy, K.V.; Singh, S. Experimental studies of TiO_2 nanoparticles synthesized by sol-gel and solvothermal routes for DSSCs application. *Results Phys.* **2019**, *14*, 102390. [[CrossRef](#)]
5. Singh, R.; Ryu, I.; Yadav, H.; Park, J.; Jo, J.W.; Yim, S.; Lee, J.-J. Non-hydrolytic sol-gel route to synthesize TiO_2 nanoparticles under ambient condition for highly efficient and stable perovskite solar cells. *Sol. Energy* **2019**, *185*, 307–314. [[CrossRef](#)]
6. Lingaraju, K.; Basavaraj, R.B.; Jayanna, K.; Bhavana, S.; Devaraja, S.; Kumar Swamy, H.M.; Nagaraju, G.; Nagabhushan, H.; Raja Naika, H. Biocompatible fabrication of TiO_2 nanoparticles: Antimicrobial, anticoagulant, antiplatelet, direct hemolytic and cytotoxicity properties. *Inorg. Chem. Commun.* **2021**, *127*, 10850. [[CrossRef](#)]
7. Chen, D.; Cheng, Y.; Zhou, N.; Chen, P.; Wang, Y.; Li, K.; Huo, S.; Cheng, P.; Peng, P.; Zhang, R.; et al. Photocatalytic degradation of organic pollutants using TiO_2 -based photocatalysts: A review. *J. Clean. Prod.* **2020**, *268*, 121725. [[CrossRef](#)]
8. Haider, A.J.; AL-Anbari, R.H.; Kadhim, G.R.; Salame, C.T. Exploring potential environmental applications of TiO_2 nanoparticles. *Energy Procedia* **2017**, *119*, 332–345. [[CrossRef](#)]
9. Lusvardi, G.; Barani, C.; Giubertoni, F.; Paganelli, G. Synthesis and characterization of TiO_2 nanoparticles for the reduction of water pollutants. *Materials* **2017**, *10*, 1208. [[CrossRef](#)] [[PubMed](#)]
10. Chen, P.C.; Chen, C.C.; Chen, S.H. A review on production, characterization, and photocatalytic applications of TiO_2 nanoparticles and nanotubes. *Curr. Nanosci.* **2017**, *13*, 373–393. [[CrossRef](#)]
11. Wang, S.; Yu, H.; Yuan, S.; Zhao, Y.; Wang, Z.; Fang, J.; Zhang, M.; Shi, L. Synthesis of triphasic, biphasic, and monophasic TiO_2 nanocrystals and their photocatalytic degradation mechanisms. *Res. Chem. Intermed.* **2016**, *42*, 3775–3788. [[CrossRef](#)]
12. Ramanavicius, S.; Ramanavicius, A. Insights in the application of stoichiometric and non-stoichiometric titanium oxides for the design of sensors for the determination of gases and VOCs (TiO_{2-x} and $\text{Ti}_n\text{O}_{2n-1}$ vs. TiO_2). *Sensors* **2020**, *20*, 6833. [[CrossRef](#)] [[PubMed](#)]
13. Zhukovskii, Y.F.; Piskunov, S.; Lisovski, O.; Bocharov, D.; Evarestov, R.A. Doped 1D nanostructures of transition-metal oxides: First-principles evaluation of photocatalytic suitability. *Isr. J. Chem.* **2017**, *57*, 461–476. [[CrossRef](#)]

14. Sidaraviciute, R.; Kavaliunas, V.; Puodziukynas, L.; Guobiene, A.; Martuzevicius, D.; Andrulevicius, M. Enhancement of photocatalytic pollutant decomposition efficiency of surface mounted TiO₂ via lithographic surface patterning. *Environ. Technol. Innov.* **2020**, *19*, 100983. [[CrossRef](#)]
15. Nosaka, Y.; Nosaka, A.Y. Generation and detection of reactive oxygen species in photocatalysis. *Chem. Rev.* **2017**, *117*, 11302–11336. [[CrossRef](#)] [[PubMed](#)]
16. Tamm, A.; Seinberg, L.; Kozlova, J.; Link, J.; Pikma, P.; Stern, R.; Kukli, K. Quasicubic α -Fe₂O₃ nanoparticles embedded in TiO₂ thin films grown by atomic layer deposition. *Thin Solid Films* **2016**, *612*, 445–449. [[CrossRef](#)]
17. Rempel, A.A.; Kuznetsova, Y.V.; Dorosheva, I.B.; Valeeva, A.A.; Weinstein, I.A.; Kozlova, E.A.; Saraev, A.A.; Selishchev, D.S. High Photocatalytic Activity Under Visible Light of Sandwich Structures Based on Anodic TiO₂/CdS Nanoparticles/Sol-Gel TiO₂. *Top. Catal.* **2020**, *63*, 130–138. [[CrossRef](#)]
18. Tuckute, S.; Varnagiris, S.; Urbonavicius, M.; Lelis, M.; Sakalauskaite, S. Tailoring of TiO₂ film crystal texture for higher photocatalysis efficiency. *Appl. Surf. Sci.* **2019**, *489*, 576–583. [[CrossRef](#)]
19. Kenmoe, S.; Lisovski, O.; Piskunov, S.; Bocharov, D.; Zhukovskii, Y.F.; Spohr, E. Water adsorption on clean and defective anatase TiO₂ (001) nanotube surfaces: A surface science approach. *J. Phys. Chem. B* **2018**, *122*, 5432–5440. [[CrossRef](#)]
20. Wunderlich, W.; Oekermann, T.; Miao, L.; Hue, N.T.; Tanemura, S.; Tanemura, M. Electronic properties of Nano-porous TiO₂- and ZnO- thin films—Comparison of simulations and experiments. *J. Ceram. Process. Res.* **2004**, *5*, 343–354.
21. Knoks, A.; Kleperis, J.; Grinberga, L. Raman spectral identification of phase distribution in anodic titanium dioxide coating. *Proc. Estonian Acad. Sci.* **2017**, *66*, 422–429. [[CrossRef](#)]
22. Brik, M.G.; Antic, Ž.M.; Vukovic, K.; Dramicanin, M.D. Judd-Ofelt analysis of Eu³⁺ emission in TiO₂ anatase nanoparticles. *Mater. Trans.* **2015**, *56*, 1416–1418. [[CrossRef](#)]
23. Nishioka, S.; Yanagisawa, K.; Lu, D.; Vequizo, J.J.M.; Yamakata, A.; Kimoto, K.; Inada, M.; Maeda, K. Enhanced water splitting through two-step photoexcitation by sunlight using tantalum/nitrogen-codoped rutile titania as a water oxidation photocatalyst. *Sustain. Energy Fuels* **2019**, *3*, 2337–2346. [[CrossRef](#)]
24. Kavaliunas, V.; Krugly, E.; Sriubas, M.; Mimura, H.; Laukaitis, G.; Hatanaka, Y. Influence of Mg, Cu, and Ni dopants on amorphous TiO₂ thin films photocatalytic activity. *Materials* **2020**, *13*, 886. [[CrossRef](#)] [[PubMed](#)]
25. Wu, F.; Hu, X.; Fan, J.; Sun, T.; Kang, L.; Hou, W.; Zhu, C.; Liu, H. Photocatalytic activity of Ag/TiO₂ nanotube arrays enhanced by surface plasmon resonance and application in hydrogen evolution by water splitting. *Plasmonics* **2013**, *8*, 501–508. [[CrossRef](#)]
26. Linitis, J.; Kalis, A.; Grinberga, L.; Kleperis, J. Photo-activity research of nano-structured TiO₂ layers. *IOP Conf. Ser. Mater. Sci. Eng.* **2011**, *23*, 012010. [[CrossRef](#)]
27. Kozlovskiy, A.; Shlimas, D.; Kenzhina, I.; Boretzkiy, O.; Zdorovets, M. Study of the effect of low-energy irradiation with O²⁺ ions on radiation hardening and modification of the properties of thin TiO₂ films. *J. Inorg. Organomet. Polym. Mater.* **2021**, *31*, 790–801. [[CrossRef](#)]
28. Mattsson, M.S.M.; Azens, A.; Niklasson, G.A.; Granqvist, C.G.; Purans, J. Li intercalation in transparent Ti-Ce oxide films: Energetics and ion dynamics. *J. Appl. Phys.* **1997**, *81*, 6432–6437. [[CrossRef](#)]
29. Dukenbayev, K.; Kozlovskiy, A.; Kenzhina, I.; Berguzinov, A.; Zdorovets, M. Study of the effect of irradiation with Fe⁷⁺ ions on the structural properties of thin TiO₂ foils. *Mater. Res. Express* **2019**, *6*, 046309. [[CrossRef](#)]
30. Kiisk, V.; Akulitš, K.; Kodu, M.; Avarmaa, T.; Mändar, H.; Kozlova, J.; Eltermann, M.; Puust, L.; Jaaniso, R. Oxygen-sensitive photoluminescence of rare earth ions in TiO₂ thin films. *J. Phys. Chem. C* **2019**, *123*, 17908–17914. [[CrossRef](#)]
31. Milovanov, Y.S.; Gavrilchenko, I.V.; Gayvoronsky, V.Y.; Kuznetsov, G.V.; Skryshevsky, V.A. Impact of Nanoporous Metal Oxide Morphology on Electron Transfer Processes in Ti–TiO₂–Si Heterostructures. *J. Nanoelectron. Optoelectron.* **2014**, *9*, 432–436. [[CrossRef](#)]
32. Reklaitis, I.; Radiunas, E.; Malinauskas, T.; Stanionytė, S.; Juška, G.; Ritasalo, R.; Pilvi, T.; Taeger, S.; Strassburg, M.; Tomašiūnas, R. A comparative study on atomic layer deposited oxide film morphology and their electrical breakdown. *Surf. Coat. Technol.* **2020**, *399*, 126123. [[CrossRef](#)]
33. Luchinsky, G.P. *Chemistry of the Titanium*; Khimija: Moscow, Russia, 1971. (In Russian)
34. Gribb, A.A.; Banfield, J.F. Particle size effects on transformation kinetics and phase stability in nanocrystalline TiO₂. *Amer. Miner.* **1997**, *82*, 717–728. [[CrossRef](#)]
35. Zhang, H.; Banfield, J.F. Thermodynamic analysis of phase stability of nanocrystalline titania. *J. Mater. Chem.* **1998**, *8*, 2073–2076. [[CrossRef](#)]
36. Hanaor, D.A.H.; Sorell, C.C. Review of the anatase to rutile phase transformation. *J. Mater. Sci.* **2011**, *46*, 855–874. [[CrossRef](#)]
37. Gupta, S.M.; Tripathi, M. A review on the synthesis of TiO₂ nanoparticles by solution route. *Cent. Eur. J. Chem.* **2012**, *10*, 279–294. [[CrossRef](#)]
38. Byranvand, M.M.; Kharat, A.N.; Fatholahi, L.; Beiranvand, Z.M. A review on synthesis of nano-TiO₂ via different methods. *J. Nanostruct.* **2013**, *3*, 1–9. [[CrossRef](#)]
39. Wang, Z.; Liu, S.; Cao, X.; Wu, S.; Liu, C.; Li, G.; Jiang, W.; Wang, H.; Wang, N.; Ding, W. Preparation and characterization of TiO₂ nanoparticles by two different precipitation methods. *Ceram. Int.* **2020**, *46*, 15333–15341. [[CrossRef](#)]
40. Wategaonkar, S.B.; Pawar, R.P.; Parale, V.G.; Nade, D.P.; Sargar, B.M.; Mane, R.K. Synthesis of rutile TiO₂ nanostructures by single step hydrothermal route and its characterization. *Mater. Today Proc.* **2020**, *23*, 444–451. [[CrossRef](#)]

41. Kusior, A.; Banas, J.; Trenczek-Zajac, A.; Zubrzycka, P.; Micek-Ilnicka, A.; Radecka, M. Structural properties of TiO₂ nanomaterials. *J. Mol. Struct.* **2018**, *1157*, 327–336. [CrossRef]
42. Sharma, A.; Karn, R.K.; Pandiyan, S.K. Synthesis of TiO₂ nanoparticles by sol-gel method and their characterization. *J. Basic Appl. Eng. Res.* **2014**, *1*, 1–5.
43. Toygun, S.; Konecoglu, G.; Kalpakli, Y. General principles of sol-gel. *J. Eng. Nat. Sci.* **2013**, *31*, 456–476.
44. Khol'kin, A.I.; Patrusheva, T.N. *Extraction-Pyrolytic Method: Fabrication of Functional Oxide Materials*; KomKniga: Moscow, Russian, 2006; ISBN 548-400-582-5. (In Russian)
45. Patrusheva, T.N.; Popov, V.S.; Prabhu, G.; Popov, A.V.; Ryzhenkov, A.V.; Snezhko, N.Y.; Morozchenko, D.A.; Zaikovskii, V.D.; Khol'kin, A.I. Preparation of a photoanode with a multilayer structure for solar cells by extraction pyrolysis. *Theor. Found. Chem. Eng.* **2014**, *48*, 454–460. [CrossRef]
46. Popov, A.I.; Shirmane, L.; Pankratov, V.; Lushchik, A.; Kotlov, A.; Serga, V.E.; Kulikova, L.D.; Chikvaidze, G.; Zimmermann, J. Comparative study of the luminescence properties of macro- and nanocrystalline MgO using synchrotron radiation. *Nucl. Instrum. Methods Phys. Res. B* **2013**, *310*, 23–26. [CrossRef]
47. Serga, V.; Burve, R.; Maiorov, M.; Krumina, A.; Skaudzius, R.; Zarkov, A.; Kareiva, A.; Popov, A. Impact of gadolinium on the structure and magnetic properties of nanocrystalline powders of iron oxides produced by the extraction-pyrolytic method. *Materials* **2020**, *13*, 4147. [CrossRef] [PubMed]
48. Burve, R.; Serga, V.; Krumina, A.; Poplausks, R. Preparation and characterization of nanocrystalline gadolinium oxide powders and films. *Key Eng. Mater.* **2020**, *850*, 267–272. [CrossRef]
49. Gindin, L.M. *Extraction Processes and Its Application*; Nauka: Moscow, Russia, 1984. (In Russian)
50. Sharlo, G. Quantitative Analysis of the Inorganic Compounds. In *Methods of the Analytical Chemistry*; Lur'e, Y.Y., Ed.; Himija: Moscow, Russia, 1969; Volume 2, ISBN 978-544-584-821-9. (In Russian)
51. Drozdov, A.A.; Zlomanov, G.N.; Mazo, G.N.; Spiridinov, F.M. Chemistry of the Transition Elements. In *Inorganic Chemistry*; Tretyakov, Y.D., Ed.; Akademija: Moscow, Russia, 2008; Volume 3, Part 1; pp. 56–99, ISBN 576-952-532-0. (In Russian)
52. Mehrotra, R.C.; Bohra, R. *Metal Carboxylates*; Academic Press: London, UK, 1983; ISBN 978-012-488-160-0.
53. Patil, K.C.; Chandrashekhar, G.V.; George, M.V.; Rao, C.N.R. Infrared spectra and thermal decompositions of metal acetates and dicarboxylates. *Can. J. Chem.* **1968**, *46*, 257–265. [CrossRef]
54. Smith, B.C. A process for successful infrared spectral interpretation. *Spectroscopy* **2016**, *31*, 14–21.
55. Stuart, B. Analytical techniques in the sciences. In *Infrared Spectroscopy: Fundamentals and Applications*; Ando, D.J., Ed.; John Wiley&Sons: Chichester, UK, 2004; ISBN 978-047-085-427-3.
56. Smith, B.C. The carbonyl group, part V: Carboxylates-coming clean. *Spectroscopy* **2018**, *33*, 20–23.
57. Nyquist, R.A.; Kagel, R.O. Infrared spectra of inorganic compounds. In *Handbook of Infrared and Raman Spectra of Inorganic Compounds and Organic Salts*, 1st ed.; Acad. Press: London, UK, 1971; pp. 1–18, ISBN 978-008-087-852-2.
58. NIST Chemistry WebBook. Available online: <http://webbook.nist.gov/chemistry/> (accessed on 2 November 2020).
59. Ocana, M.; Fornés, V.; García Ramos, J.V.; Serna, C.J. Factors affecting the infrared and raman spectra of rutile powders. *J. Solid State Chem.* **1988**, *75*, 364–372. [CrossRef]
60. Savchyn, P.; Karbovnyk, I.; Vistovskyy, V.; Voloshinovskii, A.; Pankratov, V.; Cestelli Guidi, M.; Mirri, C.; Myahkota, O.; Riabtseva, A.; Mitina, N. Vibrational properties of LaPO₄ nanoparticles in mid-and far-infrared domain. *J. Appl. Phys.* **2012**, *112*, 124309. [CrossRef]
61. Balasubramanian, C.; Bellucci, S.; Cinque, G.; Marcelli, A.; Guidi, M.C.; Piccinini, M.; Popov, A.; Soldatov, A.; Onorato, P. Characterization of aluminium nitride nanostructures by XANES and FTIR spectroscopies with synchrotron radiation. *J. Phys. Condens. Matter* **2006**, *18*, S2095–S2104. [CrossRef]
62. Bellucci, S.; Popov, A.I.; Balasubramanian, C.; Cinque, G.; Marcelli, A.; Karbovnyk, I.; Savchyn, V.; Krutyak, N. Luminescence, vibrational and XANES studies of AlN nanomaterials. *Radiat. Meas.* **2007**, *42*, 708–711. [CrossRef]